

# Influence of anodizing voltage mode on the nanostructure of TiO<sub>2</sub> nanotubes

Qunfang Gui · Dongliang Yu · Shaoyu Zhang ·  
Huapeng Xiao · Chunyan Yang · Ye Song · Xufei Zhu

Received: 23 July 2013 / Revised: 4 September 2013 / Accepted: 6 September 2013 / Published online: 15 September 2013  
© Springer-Verlag Berlin Heidelberg 2013

**Abstract** The nanostructure of self-ordered porous anodic TiO<sub>2</sub> nanotubes (PATNTs) has extraordinary influence on their physical and chemical properties. For this reason, extensive attention has been paid on pulse anodization to regulate the nanostructure of PATNT. However, the relationships between the nanostructures and current curves still remain unclear. Based on the traditional potentiostatic and pulse anodizations, five different modes (i.e., potentiostatic, pulse, triangle wave, decrease, and increase step by step) of applied voltage and their influences on the nanostructures of PATNT have been investigated in detail. The growing rates of the nanotubes anodized under five different modes were compared for the first time. The results show that the growing rate of pulse voltage anodization is the fastest, reaching 116.4 nm min<sup>-1</sup>. The slowest is triangle wave voltage anodization, only 59.3 nm min<sup>-1</sup>. When the applied voltage decreases step-by-step, branched nanotubes can be formed in the bottom of PATNT. Yet, when the applied voltage increases step-by-step, triple-layer nanotubes with different diameters are formed, and the forming mechanism of this special nanostructure is discussed. The present results may be helpful to understand the mechanism of PATNT and facilitate the assembling diverse nanostructures for extensive applications in photocatalysis, dye-sensitized solar cells, and biomedical devices.

**Keywords** TiO<sub>2</sub> nanotube · Anodization mode · Nanostructure · Electronic current

## Introduction

Porous anodic TiO<sub>2</sub> nanotubes (PATNTs) have drawn extensive attention due to their easy fabrication and various excellent optical, electrical, and biomedical properties [1–3]. It has been found that the diameter and the nanostructure of self-ordered TiO<sub>2</sub> nanotubes have extraordinary influence on their physical and chemical properties [4, 5]. Numerous efforts have been made to further increase the surface area and to change the diameter of PATNT, which is favorable for surface reactions and related applications [3–6]. For example, TiO<sub>2</sub> nanotubes with bamboo nanostructure yielded a light conversion efficiency that was 55 % higher than that of smooth-walled nanotubes with identical film thickness when used in dye-sensitized solar cells [3, 7, 8]. The bamboo-type and multilayer TiO<sub>2</sub> nanotubes assembled by pulse voltage or alternating voltage-anodizing process have received considerable attention in recent years [3, 5, 9–11]. However, the formation mechanism of bamboo-type and multilayer PATNT was not yet well understood [3, 9, 11, 12], because the pore origination on the barrier oxide layer still remains unclear [12, 13]. Moreover, as Houser and Hebert [14] indicated, the relationships between porous morphology and current–time (or voltage–time) curve still require further investigation. To the best of our knowledge, many groups have made great achievements for assembling diverse nanostructures of PATNT, but only a few researchers discussed the above relationships in detail and evaluated the growing rates of nanotubes [9, 11, 15]. Moreover, Li et al. [9] indicated that such a multilayer structure and evaluating the growing rates

Q. Gui · H. Xiao · C. Yang · X. Zhu (✉)  
School of Chemical Engineering, Nanjing University of Science and  
Technology, Nanjing 210094, China  
e-mail: zhuxufei.njust@163.com

D. Yu · S. Zhang · Y. Song (✉)  
Key Laboratory of Soft Chemistry and Functional Materials of  
Education Ministry, Nanjing University of Science and Technology,  
Nanjing 210094, China  
e-mail: soong\_ye@sohu.com

will help us to understand more deeply the formation mechanism of the PATNT.

Here, based on the traditional potentiostatic anodization and pulse anodization, we devised three new applied voltage modes (i.e., triangle wave, decrease, and increase step by step) for assembling different TiO<sub>2</sub> nanotubes. Simultaneously, the relationships between the porous TiO<sub>2</sub> nanotubes and the corresponding current–time curves have been investigated in detail; also, the nanotube growing rates of different modes have been compared. When the applied voltage decreases step-by-step, branched nanotube can be formed in the bottom of PATNT, whereas when the applied voltage increases step-by-step, triple-layer TiO<sub>2</sub> nanotubes with different diameters are formed. The forming mechanism of this triple-layer nanotubes was explained by the model of ionic current and electronic current.

## Experimental

Titanium foil (99.5 %, 0.1 mm thick, Baoji Ronghao Titanium Co., Ltd.) was polished using a mixture solution of HF (≥40 %), HNO<sub>3</sub> (65–68 %) (Shantou West Long Chemical Factory Limited), and deionized water (1:1:2 in volume) for 8–10 s. Subsequently, the samples were rinsed thoroughly by deionized water and dried in the air before anodization. The anodization was carried out in a two-electrode electrochemical cell, using the Ti foil as the working electrode and a Pt mesh as the counter electrode. The pretreated samples were all anodized in ethylene glycol (EG) solutions containing 0.3 wt% NH<sub>4</sub>F and 2 % H<sub>2</sub>O at 25 °C. Cyclic anodization was performed using Chroma Programmable DC power supply (62006P-300-8).

Two-step anodization was adopted to fabricate self-ordering PATNT. Before formal anodization, the electrolyte was aged under an anodizing voltage of 60 V for 5 h at room temperature. In the first-step anodization, the polished Ti foil was anodized at 60 V for 30 min in the aged electrolyte, and then, the as-anodized sample was ultrasonically rinsed in deionized water for 10 min to strip the formed TiO<sub>2</sub> nanotubes, getting a textured Ti substrate. After being washed and dried in the air, the as-prepared Ti substrates were anodized for the second time; the temperature and electrolyte were the same to those of the first step. However, the second-step anodization was carried out under different voltage modes, and in five different modes, the average voltage is all 40 V. The morphology of the nanotube arrays obtained from the second-step anodization was investigated. All samples were examined using a field emission scanning electron microscope (FESEM, Zeiss Supra 55 and Hitachi S-4800). Nanotube diameter was measured directly on the FESEM.

## Results and discussion

Figure 1 shows the anodizing process of the first mode and the cross-section morphology of the TiO<sub>2</sub> nanotubes. The sample was fabricated by second-step anodization under constant voltage 40 V for 30 min as a comparison. Figure 1a is a typical current density–time curve under constant voltage anodization. The inset shows three stages (I, II, and III) of pore formation and development. It is well known that these three stages correspond to three processes, i.e., the formation of the compact oxide film (stage I), the pore generation on the compact film surface (stage II), and the self-ordering process of the pore development (stage III).

Based on the traditional theories, the formation of nanotubes is governed by a competition between anodic oxide formation (reaction (1)) and chemical dissolution of the oxide as soluble fluoride complexes [TiF<sub>6</sub>]<sup>2-</sup> (reaction (2)) [1–3]. The oxide growth (reaction (1)) rate at the Ti–oxide interface

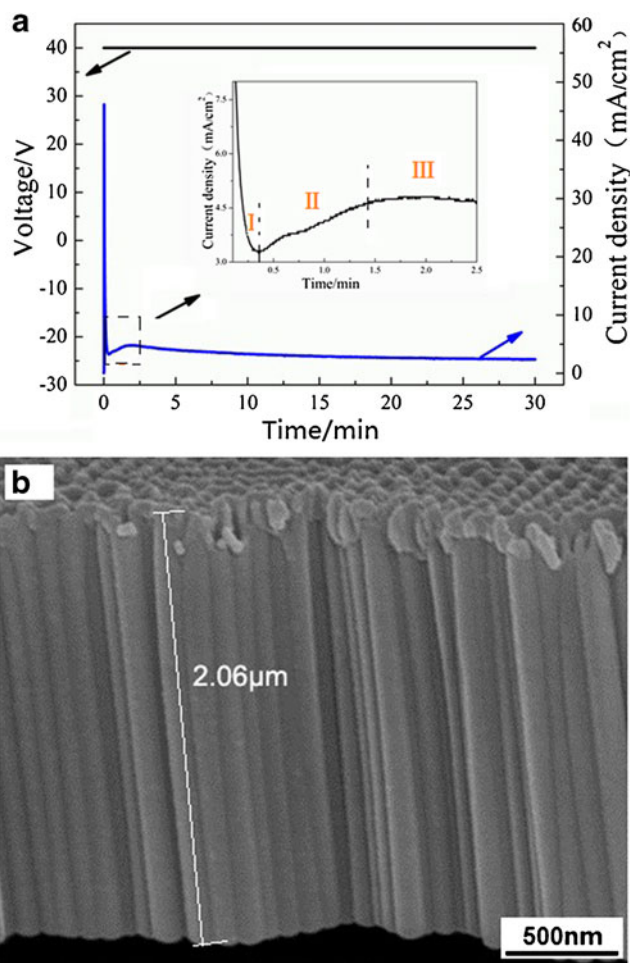
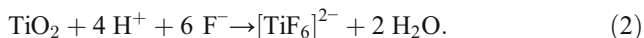
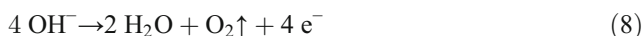
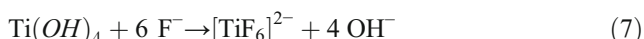
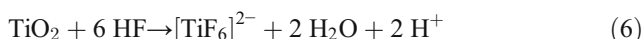


**Fig. 1** **a** Current density–time curve during the second-step anodization at 40 V for 30 min, with the *inset* showing the enlarged current density–time curve in the range of 0–2.5 min. **b** FESEM cross-section image of PATNT

and the rate of oxide dissolution (reaction (2)) at the electrolyte–oxide interface in the pore bottom ultimately become equal [2]. However, the relationship between the oxidation and dissolution reactions and the anodizing current is still unclear. That is, the explanation about the current decrease and then increase as shown in the Fig. 1a is still controversial.



For the complex electrochemical anodizing process, there are other expressions in different literatures [2, 9, 12, 16], such as:



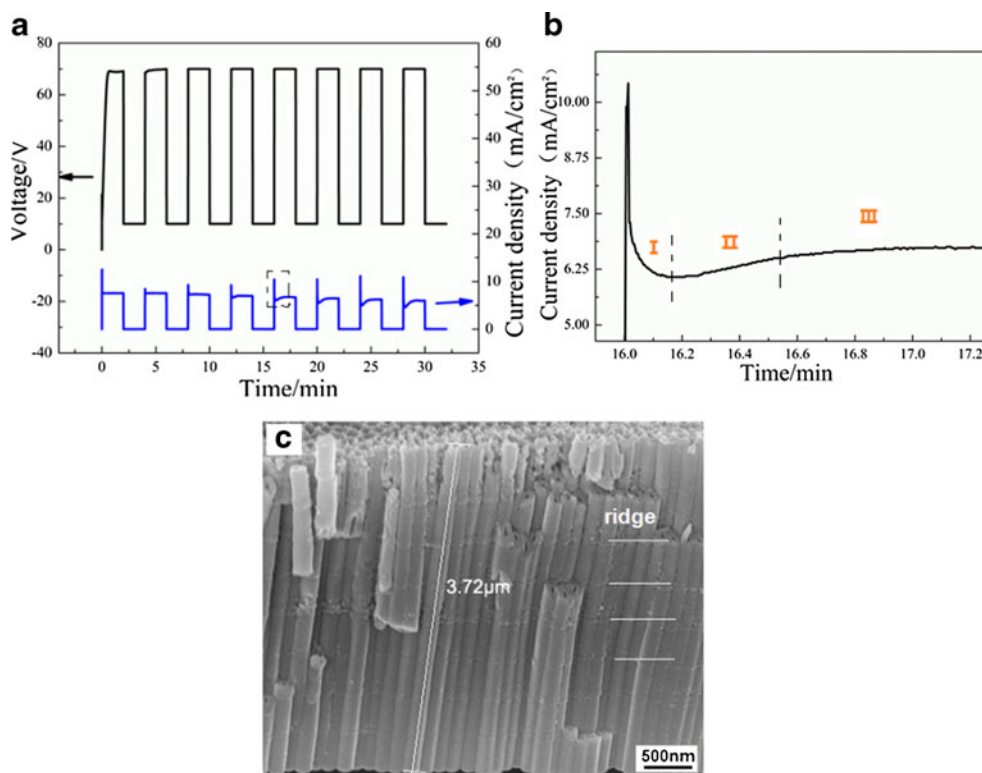
Typically, three stages of the current behavior can be ascribed to the pore initiation process. In stage I, a barrier oxide

is formed, leading to a current decay. In stage II, the surface is locally activated, and initial nanopores begin to grow. Due to the fact that barrier oxide is locally activated and dissolved, the current increases as shown in Fig. 1a. After some time, the individual pore starts interfering with each other and competing for the available current. This leads to an optimized situation where the pores equally share the available current, and self-ordering under steady state conditions is established in stage III as shown in Fig. 1a [1].

Krengvirat et al. [6] also explained why the current decreases and then increases as shown in the Fig. 1a. The rapid growth of thick barrier layer obstructed the ionic transport across the oxide, resulting in abrupt current decrease (marked as stage I in the inset of Fig. 1a). Low polarization of  $\text{Ti}^{4+}\text{-O}^{2-}$  bond in thick oxide layer retarded the pore initiation, as manifested by the gradual current increase at stage II and the shift of local minimum current to longer exposure time (marked as stage II in the inset of Fig. 1a).

Based on the competition between the reaction (1) and the reaction (2), Cao et al. [15] also proposed the oxidation current and dissolution current. The oxidation current or ionic current results in the oxide formation by reaction (1) and leads to the current decrease at stage I. The enrichment of fluoride ions at the breakdown points leads to the fast chemical dissolution of  $\text{TiO}_2$  at these locations. The current increase at stage II results from the dissolution current by reaction (2) [15].

**Fig. 2** **a** Typical voltage–time and the corresponding current density–time curve of pulse voltage anodization. **b** Magnified graph of the rectangle region marked in Fig. 2a. **c** FESEM cross-section image of PATNT



In summary, based on the chemical dissolution model [1, 2, 6, 12, 15], the ionic current or oxidation current results in the oxide growth and current decrease at stage I. The dissolution current results in the pore deepening and the current increase at stage II. However, the dissolution reaction (2) only takes place at the electrolyte–oxide interface, which cannot supply charge carriers to establish a conductive path between two interfaces (electrolyte–oxide and oxide–Ti interfaces). That is to say, the so-called dissolution current across the barrier oxide layer is impossible to be formed, because soluble product  $[\text{TiF}_6]^{2-}$  anions only enter the electrolyte and cannot pass through the barrier oxide [16]. In fact, the anodizing current density–time curve reflects the total current throughout the anodic oxide film.

As Liu et al. [2] indicated that the nanotube growth rate depends on either solid-state transport of ions through the oxide barrier layer or the availability of ionic species at the oxide–electrolyte interface. Meanwhile, the movement of the metal cations and oxygen ions is related to the ionic current [2]. We have investigated the metal-anodizing processes and their anodizing current–time curves in our previous works [16–18]. The total anodizing current mainly includes ionic current and electronic current during anodizing process. The ionic current is used to form the barrier oxide, and the electronic current is used to give rise to oxygen gas (the above reactions (8) or (9)) [16–18], and then, the evolution and development of  $\text{TiO}_2$  nanotubes arise from the viscous flow of the barrier oxide around the oxygen bubble from the bottom toward the cell walls [14, 19, 20]. This viewpoint has received considerable attention and citation [21–24]. Herein, a new explanation about the three stages is given. At first, the curve appears to be an exponential drop, the barrier oxide forms quickly due to the high electric field strength and ionic conduction. The ionic current reaches to the minimum value at stage I as shown in Fig. 1a, which means that the barrier oxide gets to the critical thickness. Subsequently, the anodizing current also begins to rise at stage II as shown in Fig. 1a, due to the generation of electronic current and the formation of the oxygen bubble mold [16]. The initial nanopores begin to generate because of the oxygen bubble mold [16–18]. Finally, the anodizing current becomes stable at a certain value, because the ionic current and electronic current tend to be constant at the critical thickness of the barrier layer [16, 17].

Figure 1b shows the cross-section morphology of the nanotubes, and the smooth-walled nanotubes are presented. To better understand the influence of the anodization voltage on the  $\text{TiO}_2$  nanotubes, the thickness of which was measured directly in the FESEM images. From Fig. 1b, as we can see, the total thickness of nanotubes fabricated under 40 V is  $2.06 \mu\text{m}$ , and as can be calculated, the average growing rate is  $68.3 \text{ nm min}^{-1}$ .

The second anodization mode with pulse voltage was investigated. Figure 2 shows the voltage–time and the

current–time curves and the corresponding nanotubes. The nanotubes were fabricated under alternating voltage condition with a sequence of 2 min at 70 V and 2 min at 10 V for 8 cycles; the total time is 32 min, which can be seen from the upper part of Fig. 2a, and the lower part is the corresponding output current density–time curve, and its shape is much like the voltage–time curve. When the voltage returns to 70 V from 10 V, there is an instant current increase. However, the current quickly drops and then keeps stable, as shown in stages I, II, and III of Fig. 2b; this indicates that the oxide film becomes firstly thick and, afterwards, thin [11], and if the voltage of 10 V is applied for a sufficient time, small tubes can be formed [3]. Here, the three stages in Fig. 2b are very similar to those in Fig. 1a. If the three stages of the current behavior (Fig. 2b) correspond to a new pore-initiating process, there are eight pore-initiating processes in Fig. 2a. However, eight pore-initiating processes are completely unnecessary. The anodizing current increase and decrease as shown in Fig. 2b result from the different voltages (70 and 10 V), leading to the different ionic currents and electronic currents at the corresponding critical thickness at the pore bottoms [18]. That is,

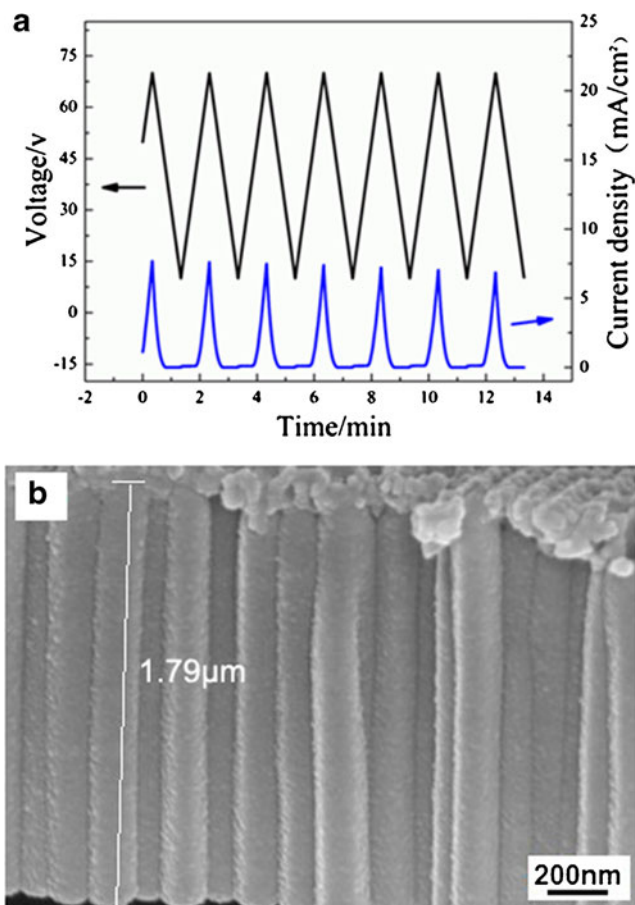


**Fig. 3** **a** Typical voltage–time and the corresponding current density–time curve during the anodization of Ti foil under the triangle wave voltage. **b** FESEM cross-section image of PATNT

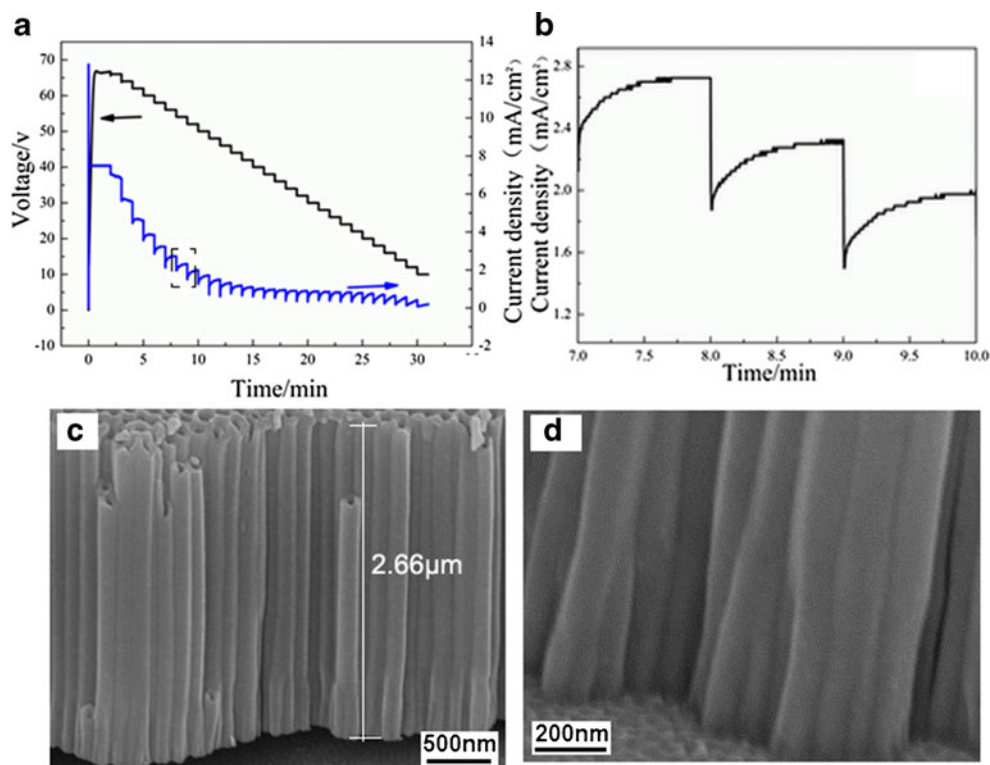
the anodizing currents at 10 and 70 V are very different as shown in Fig. 2a. The anodizing current is about  $6.5 \text{ mA cm}^{-2}$  at 70 V for 30 min, and the anodizing current reduces to about 0 at 10 V for 30 min. The ionic current and electronic current under an applied voltage of 10 V are very low, because the critical thickness of the barrier layer is corresponding to the peak voltage 70 V, and this critical thickness becomes too thick for 10 V.

Figure 2c reveals the obtained bamboo-type nanotubes which possess rough walls because of the extra ridges around the nanotubes. The current–time curve in Fig. 2a shows much smaller anodic current at low-voltage steps than at high-voltage steps. As we know, the ridge spacing and nanotube length mainly depend on high-voltage anodization rather than low-voltage anodization. Meanwhile, the role of low-voltage step is to gather more electrolytes into the gaps around the nanotubes, and then, the circle ridge is formed at the electrolyte–Ti interface due to the high ionic current at the high voltage of 70 V. The thick barrier at the pore bottom and the circle ridge around the nanotubes all result from the high ionic current peak as shown in Fig. 2b. Therefore, each nanotube seems to be divided into eight parts as shown in Fig. 2c, and seven ridges can be found. As can be calculated, the average growing rate is  $116.4 \text{ nm min}^{-1}$ .

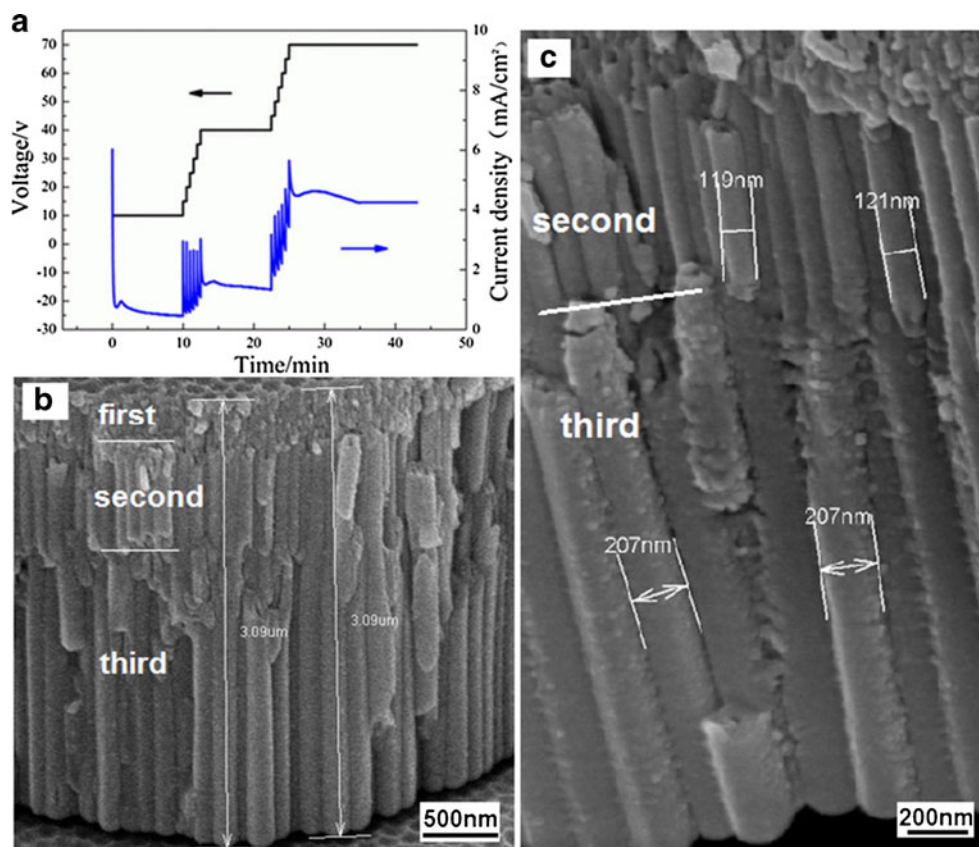
The third anodization mode was carried out under a triangle-wave voltage. Figure 3 shows the voltage–time curve, current density–time curve, and the corresponding nanotubes. In this case, the high and low voltage is also 70 and 10 V,

respectively. The anodizing voltage increases and decreases both at a rate of  $1 \text{ V s}^{-1}$ , and the total time is 30 min. As can be seen from Fig. 3a, the current density output is slightly deformed from the expected triangular shape. The current density–time curve (Fig. 3a) shows a slight reduction in the current density during the anodization process. Such reduction in current density over time is due to the reduction of ion exchange efficiency with the growing of the nanotubes [25]. In the electrochemical reaction, forming the  $\text{TiO}_2$  nanotubes involves the participation of ions in the solution, especially the  $\text{O}^{2-}$  and  $\text{F}^-$ . When the nanotubes are growing, it becomes increasingly difficult for the anions in the electrolyte to reach the tube bottom. Consequently, with the growing of nanotubes, the current density will decrease if the anodizing voltage remains unchanged. This phenomenon also can be found in Figs. 1a and 2a. Figure 3b shows the cross-section morphology of nanotubes. The smooth-walled nanotube morphology as shown in Fig. 3b is totally different from that of PATNT reported by Xie et al., while they used the same method and assembled the bamboo-like nanotubes [25]. As can be calculated, the average growing rate is  $59.3 \text{ nm min}^{-1}$ . When the voltage is less than 41 V, the barrier layer (corresponding to voltages higher than 41 V) is too thick, and the electric field becomes too weak to generate ionic conduction; the ionic current and electronic current are approximately  $\sim 0 \text{ mA}$  as shown in Fig. 3a, which cannot support the nanotube growing, so the average growing rate under this mode is the lowest in this paper.

**Fig. 4** **a** Typical voltage–time curve and the corresponding current density–time curve. **b** Magnified graph of the rectangle region marked in Fig. 4a. **c** FESEM cross-section image of PATNT. **d** Magnified cross-section image of PATNT to observe branched nanotubes



**Fig. 5** **a** Typical voltage–time curve and the corresponding current density–time curve. **b** FESEM cross-section image of PATNT. **c** Magnified image showing the diameters of the nanotubes in the second and third layers



The fourth mode was investigated via the progressive reducing anodizing voltage method. Figure 4 shows the voltage–time curve, current density–time curve, and the corresponding nanotubes. This anodization is under the condition that the applied voltage decreases by 2 V each time from 70 to 10 V, and each voltage stays for 1 min (Fig. 4a). From Fig. 4b, we can see that the current quickly drops and then keeps stable, which is the same with Fig. 2b. When the applied voltage decreases to ~45 V, the current density has a steep drop. Such phenomenon can be attributed to the ceaseless decreasing voltage across the thick barrier layer, causing the ionic current and electronic current to drop to a rather low value. As shown in Fig. 4c, the nanotubes have become branched, because the barrier layer becomes thin, and nanotube diameter becomes small with the voltage decrease. The diameter of the upper nanotubes is much larger than that of the lower branched nanotubes, which is clearly illustrated in Fig. 4d. As can be calculated, the average growing rate is 88.3 nm min<sup>-1</sup>.

The fifth mode was investigated via a raising anodizing voltage method shown in Fig. 5a. Figure 5 shows the voltage–time curve, current density–time curve, and corresponding nanotubes. PATNT was fabricated under first 10 V and then 40 V and, finally, 70 V; each applied voltage stays for 10 min. The voltage increases by 5 V each time from 10 to 40 V and from 40 to 70 V, and each small step for voltage increase

maintains for 30 s (Fig. 5a), which is good for nanotube growing. The lower curve is the corresponding current density–time curve in Fig. 5a. When the applied voltage is 10 V, the current density is especially low as shown in Fig. 5a.

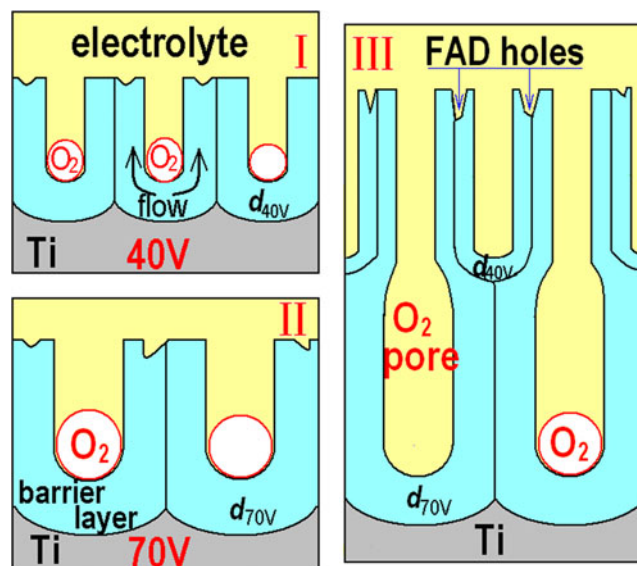


**Fig. 6** Schematic diagram showing the formation of two-layer nanotubes under different voltages (40 and 70 V)

Figure 5b shows the triple-layer nanotube array. The diameter of nanotubes in each layer is proportional to their corresponding anodizing voltage 10, 40, and 70 V, respectively. As shown in Fig. 5c, in the first layer, the nanotube diameter is only ~40 nm, which is mainly because of the low applied voltage. The nanotube diameter of the second and third layer is ~120 and ~207 nm, respectively. Though each step of applied voltage (10, 40, and 70 V) is all held for 10 min, the layer lengths are diverse due to different voltages. That is to say, within the same time period, more quantity of electric charge is transferred at a high-voltage step than at a low-voltage step. According to the current density–time curve in Fig. 5a, the average current density corresponding to the three steps is 0.63, 1.46, and 4.38 mA cm<sup>-2</sup>, respectively, and the nanotube length of each layer corresponding to the three steps is ~300, ~800, and ~1,900 nm, respectively. This illustrates that the nanotube length is basically in proportion to the current density, but not to the applied voltage. As can be calculated, the average growing rate is 96.6 nm min<sup>-1</sup>.

As shown in Fig. 5b, we suppose that the number of nanotubes in the first, second, and third layers is  $n_1$ ,  $n_2$ , and  $n_3$ , respectively, and then obviously,  $n_1 > n_2 > n_3$ , but this phenomenon cannot be explained by chemical dissolution (reaction (2)) or field-assisted dissolution (FAD) model [18]. According to FAD model, the nanopores of the second layer will develop in the foundation of the first layer, and that means,  $n_1 = n_2 = n_3$ , but the truth is not so. We have concluded that different applied voltages would lead to the change of ionic current in the same electrolyte [16]. In this paper, higher applied voltage mainly results in the increase of ionic current as shown in Fig. 5a, so the barrier layer will be thicker with the increase of applied voltage. When the applied voltage increases, the critical thickness ( $d$ ) of the barrier layer also increases (obviously  $d_{10\text{ V}} < d_{40\text{ V}} < d_{70\text{ V}}$ ), in which the electronic current generates, and the oxygen bubble mold forms. Based on the flow model [14, 18–20], the thicker the barrier layer flows around the oxygen bubble mold, the thicker nanotube wall is formed around the bubble mold. Then, the number of nanotubes decreases, and nanotube diameter increases with the applied voltage increase. This explanation corresponds to the conclusion proposed by Yasuda and Schmuki [4]. When the potential is altered between anodization steps, the diameter of the nanotubes can be changed [4]. This behavior has also been reported by Yang et al. [5]. They assembled TiO<sub>2</sub> nanotubes under the anodizing voltage of 5 V for 2 h and 15 V for 2 h, respectively. The obtained nanotube arrays were clearly separated into two layers with different diameters [5], just as the first and second layer shown in Fig. 5b. The diameter of the nanotubes increases with the applied voltage [4, 9]. A detailed discussion about the diameter with the voltage was reported in our recent work [26]. Here, Fig. 6 shows the schematic diagram of the formation process of two-layer nanotubes.

## Conclusions

In summary, when different anodizing voltage modes are applied, there are remarkable differences about the cross-section images of obtained TiO<sub>2</sub> nanotubes. While taking into account the current density–time curves, we can have a deep comprehension of the formation of PATNT. Though the average voltage of five modes is all 40 V, the growing rates vary greatly, which are 68.3, 116.4, 59.3, 88.3, and 96.6 nm min<sup>-1</sup>, respectively. When the applied voltage increases, the critical thickness of the barrier layer also increases, in which the electronic current generates, and the oxygen bubble mold forms. The formation process of triple-layer nanotubes can be clarified by the combination of flow model with the oxygen bubble mold. The present results may be helpful to understand the mechanism of PATNT and facilitate assembling diverse nanostructures for extensive applications in photocatalysis, dye-sensitized solar cells, and biomedical devices.

**Acknowledgments** This work was financially supported by grants from the National Natural Science Foundation of China (grant nos. 61171043 and 51077072).

## References

- Macak JM, Tsuchiya H, Ghicov A, Yasuda K, Hahn R, Bauer S, Schmuki P (2007) *Curr Opin Solid St M* 11:3–18
- Liu G, Hoivik N, Wang K, Jakobsen H (2012) *Sol Energy Mater Sol Cells* 98:24–38
- Guan DS, Wang Y (2012) *Nanoscale* 4:2968–2977
- Yasuda K, Schmuki P (2007) *Electrochem Commun* 9:615–619
- Yang D, Park H, Kim H, Cho S, Choi W (2009) *J Electroceram* 23: 159–163
- Krengvirat W, Sreekantan S, Noor AFM, Kawamura G, Muto H, Matsuda A (2013) *Electrochim Acta* 89:585–593
- Kim D, Ghicov A, Albu SP, Schmuki P (2008) *J Am Chem Soc* 130: 16454–16455
- Luan XN, Guan DS, Wang Y (2012) *J Phys Chem C* 116:14257–14263
- Li HY, Wang JS, Huang KL, Sun GS, Zhou ML (2011) *Mater Lett* 65:1188–1190
- Liu Y, Wang DA, Cao LX, Chen SG (2012) *Electrochem Commun* 23:68–71
- Guan DS, Hymel PJ, Wang Y (2012) *Electrochim Acta* 83:420–429
- Su ZX, Zhou WZ (2011) *J Mater Chem* 21:8955–8970
- Hebert KR, Albu SP, Paramasivam I, Schmuki P (2012) *Nat Mater* 11:162–166
- Houser JE, Hebert KR (2009) *Nat Mater* 8:415–420
- Cao CB, Li JL, Wang X, Song XP, Sun ZQ (2011) *J Mater Res* 26: 437–442
- Zhu XF, Song Y, Liu L, Wang C, Zheng J, Jia H, Wang X (2009) *Nanotechnology* 20:475303, 7pp
- Yang RQ, Jiang LF, Zhu XF, Song Y, Yu DL, Han A (2012) *RSC Adv* 2:12474–12481
- Zhu XF, Song Y, Yu DL, Zhang C, Yao W (2013) *Electrochem Commun* 29:71–74

19. LeClere DJ, Velota A, Skeldon P, Thompson GE, Berger S, Kunze J, Schmuki P, Habazaki H, Nagata S (2008) *J Electrochem Soc* 155: C487–C494
20. Li DD, Zhao LA, Jiang CH, Lu JG (2010) *Nano Lett* 10:2766–2771
21. Ispas A, Bund A, Vrublevsky I (2010) *J Solid State Electrochem* 14: 2121–2128
22. Paternaraki G, Diakonikolaou J (2012) *J Solid State Electrochem* 16:2921–2939
23. Li Y, Ling ZY, Hu X, Liu YS, Chang Y (2012) *RSC Adv* 2:5164–5171
24. Pauric AD, Baig SA, Pantaleo AN, Wang Y, Kruse P (2013) *J Electrochem Soc* 160:C12–C18
25. Xie YL, Li ZX, Xu H, Xie KF, Xu ZG, Zhang HL (2012) *Electrochem Commun* 17:34–37
26. Yu DL, Song Y, Zhu XF, Yang RQ, Han AJ (2013) *Appl Surf Sci* 276:711–716